Green synthesis, characterization and biological activity of synthesized ruthenium nanoparticles using fishtail fern, sago palm, rosy periwinkle and holy basil

Pranshu K. Gupta[1], Kalluri V. S. Ranganath[1], Nawal K. Dubey[2] and Lallan Mishra[1,*]

[1]Department of Chemistry, and
[2]Department of Botany, Institute of Science, Banaras Hindu University, Varanasi 221 005, India

Ruthenium nanoparticles (Ru NPs) of different sizes prepared using leaf extracts of fishtail fern (*Nephrolepis biserrata*), sago palm (*Cycas revoluta*), rosy periwinkle (*Catharanthus roseus*) and holy basil (*Ocimum tenuiflorum*) in methanol exhibited pronounced antifungal (against *Aspergillus flavus*) and antioxidant activity (DPPH, ABTS, SO, OH). The synthesized Ru NPs were characterized using FTIR, UV-visible spectra, fluorescence and XRD. A tentative synthetic mechanism of NPs has been hypothesized via redox mechanism. A correlation between size of nanoparticles and plant groups has also been established.

Keywords: Antifungal, antioxidant, biosynthesis, nanoparticles, ruthenium.

GREEN synthesis of nanoparticles (NPs) has attracted attention owing to its environment friendly protocol[1–3]. Synthesis of novel NPs of Ag, Au, Pt, Pd and Ru with special chemical and biological functions, tuned shape and size and dispersity, has been quite interesting. It is demanding to avoid the use of toxic chemicals[4]. In this context, plant extracts have turned out to be the best alternatives to synthesize NPs in view of their good yield and significant biological activity. In this direction, many plant extracts had been used for synthesis of metal and metal-oxide NPs[5–9].

Among the metals, ruthenium (Ru), being a low cost material as compared to Pd and Pt, has been exhaustively used in catalytic dehydrogenation[10], diesel fuel generation[11], azo dye degradation[12], antiorgano-pollutants[13] and redox catalysis[14]. Ru NPs have been synthesized using different chemical methods including reduction of Ru salts in aqueous medium by a strong chemical reducing agent, or by thermolysis in refluxing alcohols[15]. The Ru NPs developed on various supports have been used in hydrogen evolution reaction and hydrogenation reactions, dye degradations[16–19].

*For correspondence. (e-mail: lmishrabhu@yahoo.co.in)

However, these methods have been reported to dump toxic chemicals and solvents imposing a threat to environment and human lives. Hence, development of a new and 'green' protocol for synthesis of NPs is an alternative. Hydrothermal synthesis provides higher yields and monodispersity[20] in comparison with microwave assisted and other protocols. These methods although 'greener and applicable', required energy, chemicals and consumed power, and hence were expensive.

Plant extract mediated metal NPs synthesis is studied and exploited for biological activity[21]. However, only few reports are available regarding microbe mediated synthesis of Ru NPs using *Pseudomonas aeruginosa* SM1[22], *Dictyota dichotoma*[23]; and plant extract mediated synthesis of Ru and RuO_2 NPs by using *Gloriosa superba*[24], *Acalypha indica*[25]. Bimetallic Ru-Pt nano-catalysts employing *Diospyros kaki* leaf extract has also been synthesized[26]. The antifungal and antioxidant properties of Ru NPs have not yet been reported to the best of our knowledge.

In the present study, *Ocimum sanctum* Linn (common name: holy basil, tulsi), also called *Ocimum teniflorum*, a member of Angiosperm[27]; *Catharanthus roseus* Linn. (common name: rosy periwinkle, Sadabahar) also called *Vinca rosea*, a member of Angiosperm[28]; *Cycas revoluta* (common name: sago palm), a gymnosperm[29]; *Nephrolepis biserrata* Sw. *Furcans* (common name: fishtail fern), a member of pteridophyta[30], were selected for the synthesis of Ru NPs, followed by chemical and biological characterization of these NPs. These selected plants are well established in chemical compositions and have significant therapeutic properties[27–30]. An attempt has also been made to formulate a tentative, redox type, mechanism in the synthesis of Ru NPs. As a surmise, NPs with more surface are a must show enhanced biological activity which varies amongst plants, specially plants known for better disease enduring abilities and generating more stress-tolerant NPs than others, irrespective of their particle size or any other biophysical factor. Moreover, particle size versus biological activity

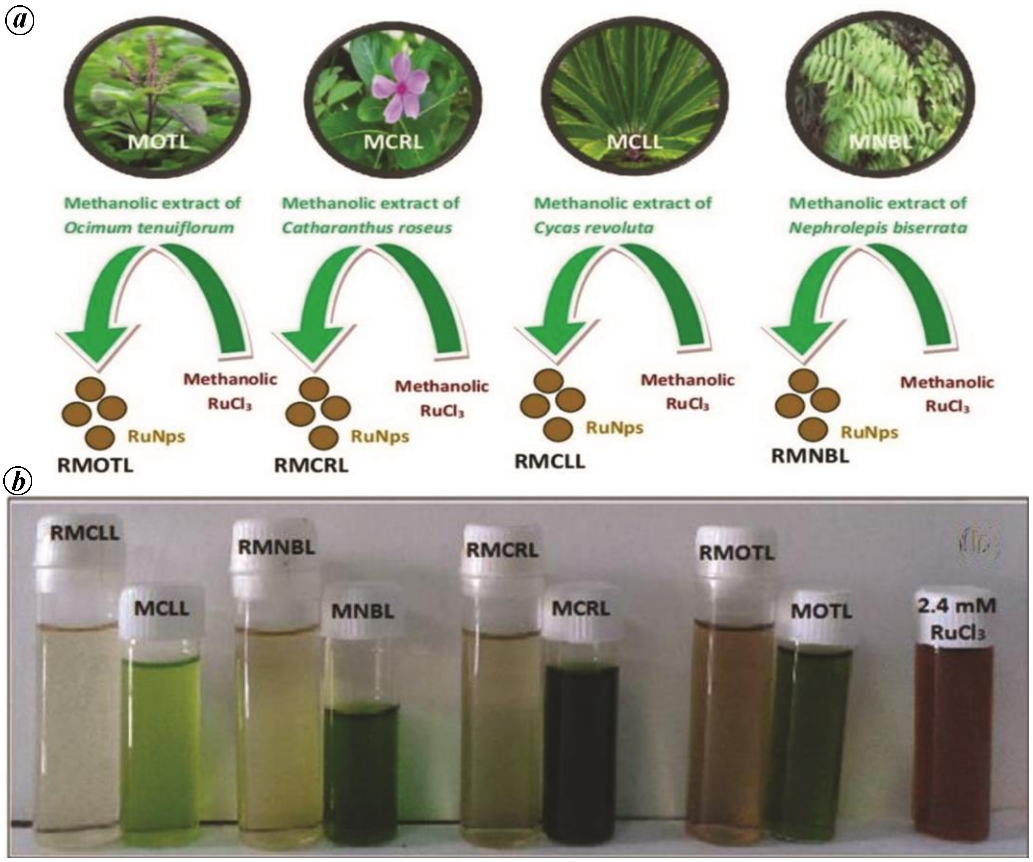

Figure 1. Illustration of synthesis of Ru NPs. ***a***, Synthetic strategy for Ru NPs. ***b***, Ru NPs synthesized from plant extracts. The synthesized NPs showed pale yellow colour which could be distinguished from that of 2.4 mM $RuCl_3$ solution. In the figure, each of the synthesized NPs (RMCLL, RMNBL, RMCRL and RMOTL) were preceded by their respective plant extracts (MCLL, MNBL, MCRL and MOTL).

plots or nanoparticle-plant group (NP-Pg) correlation plots are also developed in the present study.

Synthesis protocol

Ruthenium chloride [$RuCl_3 \cdot xH_2O$], procured from Sigma-Aldrich was directly used without further purification. Leaves of plants (*Catharanthus roseus*, *Ocimum tenuiflorum*, *Cycas revoluta* (male) and *Nephrolepis biserrata*) were collected from Botanical Garden, Department of Botany, Banaras Hindu University, Varanasi, India. The collected leaves were thoroughly washed with double distilled water for about three times and then air dried. Fresh and finely cut leaves (≈5.0 g) of each of the plants namely, *Catharanthus roseus* (MCRL), *Ocimum tenuiflorum* (MOTL), *Cycas revoluta* (MCLL) and *Nephrolepis biserrata* (MNBL), were boiled in an autoclaved 100 ml Erlenmeyer flask with 40 ml methanol, at 50°C, for about 10 min. The extracts were then filtered separately, first through a muslin cloth and then through Whatmann No. 1 filter paper. The filtrates were collected in a separate autoclaved flask and stored in refrigerator at 4°C for further experiments and investigations. Fresh plant extracts were employed, for each synthesis.

About 40 ml, 2.4 mM, wine red methanolic solution of ruthenium chloride ($RuCl_3 \cdot xH_2O$), was instantly prepared for the synthesis of each of the Ru NPs, in four different Erlenmeyer flasks (250 ml) and each of them were stirred at 1200 rpm, at 50°C, for 5 min, on a sand bath. After 5 min, 500 µl of MCRL, MCLL, MNBL and MOTL plant extracts were added separately to each flask. The reaction was continued for all under similar conditions for about 30 min. The synthesis of Ru NPs was marked by a visible colour change of the reaction from wine red to light yellow and further monitored by UV-Visible spectroscopy. These four solutions were vortexed and then the synthesized NPs were collected by centrifugation at 17,800 rpm for 15 min. The NPs were then collected under minimum methanol and stored at room temperature. The four different Ru NPs so synthesized were labelled as RMCRL, RMCLL, RMNBL and RMOTL and their general synthesis is shown in Figure 1.

Characterization

The synthesis of Ru NPs was confirmed (in liquid media itself) by UV-Visible spectroscopy, in the wavelength

range of 200–800 nm, using Shimadzu spectrophotometer (model UV-1800) operated at a resolution of 1 nm. The methanolic solutions of Ru NPs were dried using rota-vapour and vibration spectroscopic studies were performed, using Varian 3300 Fourier Transform Infrared Spectroscopy (FTIR) carried in the wavelength range of 400–4000 cm^{-1}. The fluorescence studies were carried out using the liquid samples of Ru NPs, through Elico SL 174 spectrofluorometer, within 400–500 nm wavelength range. X-Ray diffraction patterns were recorded from drop coated films of Ru NPs on glass substrate, using Cu K_α radiation ($\lambda = 0.154060$ nm), with Ni monochromatic, within 10° to 80°, 2θ range. Various crystal parameters were calculated and average crystallite size was accurately calculated by Debye Scherrer's formula[31]. Size, composition and morphology of Ru NPs were further analysed by scanning electron microscopy (SEM). Energy dispersive X-ray spectroscopy (EDX) was performed by preparing a thin film of Ru NPs by spin coating (1500 rpm) method, applied on a clean aluminium foil (1 cm × 1 cm) and dropping approximately 100 µl of sample that was allowed to dry for 30–40 min, at room temperature, and subjecting it to SEM instrument (model: FEI Quanta 250). Particle size was accurately determined using a JOEL 1200 EX-2010 transmission electron microscope (TEM) operating at 200 kV. This was pre-equipped with SAED analyser Cu grid which was coated by Ru NPs and then TEM was done.

Biological activities of biosynthesized Ru NPs were investigated by performing antifungal assays as well as antioxidative studies such as 2,2′-diphenyl-1-picrylhydrazyl (DPPH), 2,2′-azino-*bis*-(3-ethylbenzthiazoline-6-sulphonic acid) (ABTS), superoxide (SO) and hydroxyl (OH) scavenging assays.

The antifungal activity (AFA) of Ru NPs was studied against *Aspergillus flavus* employing food poisoning technique as stated by Balouiri[32], with some modifications. Fungal strain was provided with food bearing Ru NPs to check their growth. Furthermore, the results were compared with a similar set-up containing plant extracts instead of Ru NPs. Under sterilized conditions of horizontal flow laminar cabinet, disks of freshly cultured fungus were placed at the centre of 10 ml PDA (potato dextrose agar) plates, each bearing different amounts of Ru NPs ranging between 200, 400, 600 and 800 µl. The same strategy was employed for all different Ru NPs as well as for plant extracts (amount ranging between 100, 500 and 1000 µl). The culture plates were allowed to incubate at 27°C, for seven days in a biological oxygen demand (BOD) incubator.

DPPH radical scavenging assay was employed to investigate the antioxidant activity of plant extracts, as well as biosynthesized NPs following the protocol similar to that of Blois and team[33]. About 500 µl of 0.2 mM methanolic DPPH solution was added to 500 µl of each of the methanolic biosynthesized Ru NPs (0.1–1.0 mg/ml), 500 µl of methanol (as control), and to 500 µl of each of methanolic ascorbic acid solution (0.1–1.0 mg/ml) (as standard). After 30 min, absorbance of these solutions was measured at 517 nm. On the basis of the absorbance data of Ru NPs ($A_{\text{Ru NPs}}$) and of control (A_{control}), the percentage of DPPH scavenging (%DPPH) was estimated, using the equation

$$\%\text{DPPHS} = \frac{A_{\text{control}} - A_{\text{Ru NPs}}}{A_{\text{control}}}. \quad (1)$$

The antioxidant activity was further estimated by a more sensitive ABTS radical scavenging assay following protocol of Re *et al.*[34]. The 7 mM ABTS and 2.4 mM potassium persulphate stock solutions were prepared separately, and equal volumes of both solutions, were mixed to prepare working solution. This was allowed to react for 12 h at room temperature in dark. The solution was then diluted by mixing its 1.0 ml with 60 ml methanol to obtain an absorbance of 0.706 ± 0.001 units at 734 nm using spectrophotometer. Fresh ABTS solution was prepared for each assay. Ru NPs solutions (2.0 ml) were allowed to react with 2 ml of the ABTS solution and the absorbance was taken at 734 nm after 7 min using spectrophotometer. The scavenging activity of each of the Ru NPs was investigated over a solution range of 0.1–1.0 mg/ml. The ABTS scavenging capacity of Ru NPs were compared with that of butylated hydroxytoluene (over the range of 0.1–1.0 mg/ml), as standard, and per cent ABTS scavenging (%ABTSS) calculated from the absorbance data of butylated hydroxytoluene as control (without Ru NPs), and of Ru NPs, i.e. $A_{\text{Ru NPs}}$ and A_{control} respectively, with the equation

$$\%\text{ABTSS} = \frac{A_{\text{control}} - A_{\text{Ru NPs}}}{A_{\text{control}}}. \quad (2)$$

The Superoxide Radical Scavenging (SORS) activity was tested by performing the superoxide radical scavenging assay following Robak and Gryglewski[35]. The reduction occurred in the presence of NBT (4-nitro blue tetrazolium chloride) with non-enzymatic phenazine methosulphate-nicotinamide adenine dinucleotide (PMS/NADH) generated superoxide radicals that reduced the blue coloured NBT to purple red colour. Different concentrations of each of 500 µl methanolic Ru NPs (0.5–1.0 mg/ml), and 500 µl of water (as control), were added to 500 µl of nicotinamide adenine dinucleotide (NADH) (156 µM) and 500 µl of NBT (630 µM) in 1.3 ml of 0.1 M phosphate buffer (pH 7.4). The reference solution contained quercetin, 500 µl of NBT (630 µM) in 2.3 µl of 0.1 M phosphate buffer (pH 7.4). The reaction was started after addition of 500 µl methylphenazonium methosulphate (PMS) (30 µM) to all mixtures. After 5 min, absorption was measured at 560 nm. Thereafter, per cent inhibition

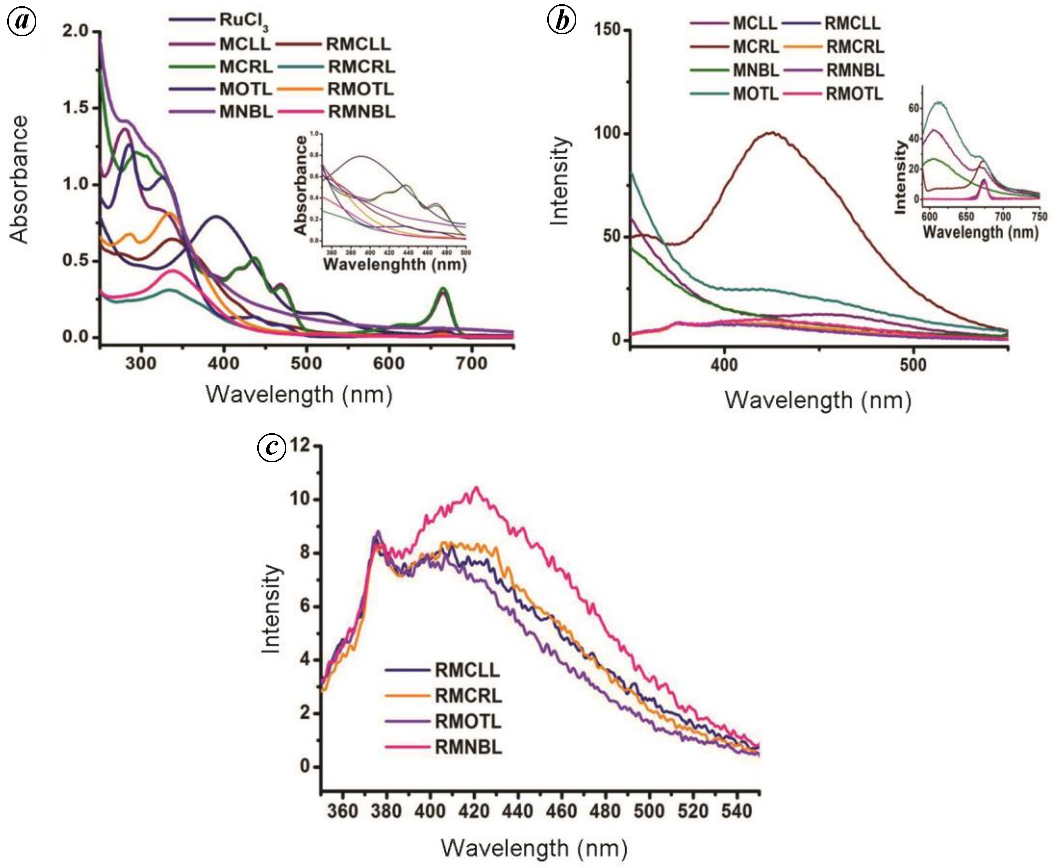

Figure 2. Absorption and emission spectra of Ru NPs. ***a***, Represents the combined UV-Visible spectra of all the plant extracts and their respective NPs. ***b***, Represents the combined fluorescence spectra of the plant extracts and their respective Ru NPs. ***c***, Represents the combined fluorescence spectra of all Ru NPs.

of superoxide radical (%ISA) was calculated from the absorbance data of mannitol as control (without Ru NPs), and of Ru NPs, i.e. $A_{\text{Ru NPs}}$ and A_{control} respectively, by using the equation

$$\%\text{SORS} = \frac{A_{\text{control}} - A_{\text{Ru NPs}}}{A_{\text{control}}}. \quad (3)$$

The OH^- scavenging activity (HSA) was measured using Fenton's reaction[36]. Reaction mixture contained 60 µl of 1.0 mM $FeCl_3$, 90 µl of 1 mM 1,10-phenanthroline, 2.4 ml of 0.2 M phosphate buffer (pH 7.8), 150 µl of 0.17 M H_2O_2, and 1.5 ml of each of Ru NPs at different concentrations (0.1–1.0 mg/ml). The aliquots were incubated at room temperature for 5 min, after which their absorbance was recorded at 560 nm. The per cent inhibition of hydroxyl radicals (%IHR) was calculated from the absorbance data of control (without Ru NPs), and of Ru NPs, i.e. $A_{\text{Ru NPs}}$ and A_{control} respectively, using the following equation and compared with mannitol as standard

$$\%\text{HSA} = \frac{A_{\text{control}} - A_{\text{Ru NPs}}}{A_{\text{control}}}. \quad (4)$$

The reduction of $RuCl_3$ in the presence of different extracts was identified by visible colour changes from wine red colour (of $RuCl_3$) to dim yellow at 50°C, after 30 min of stirring at 1200 rpm, indicating the formation of Ru NPs of size ~25 nm. The prepared NPs were highly stable over two months.

Results and discussion

The preliminary confirmation of Ru NPs has been done by UV-Visible spectroscopy, within 250–700 nm wavelength range at λ_{max} of 240 nm. Four Ru NPs solutions, along with four plant extracts and one $RuCl_3$ solution were diluted over a decade using methanol and their absorption peaks were recorded. Figure 2 *a*, shows the combined UV-Visible spectra of all the nine samples. $RuCl_3$ solution shows a broad peak at 391 nm and a narrow one at 524 nm. Colloidal suspension of Ru NPs depicts characteristic exponential decay pattern, without any absorption peak[37]. Similar absorption patterns were observed for all four plant extracts, with absorption maxima of chlorophyll (338 nm, 665 nm), and carotenoids such as lutein and β-carotene (~415 nm, 438 nm, 468 nm)[38]. UV-Visible spectra of Ru NPs showed no peaks of $RuCl_3$ (390 nm, 524 nm). However, low intensity peaks (~338, 665 nm) of carotenoids (~415 nm, 438 nm, 468 nm)

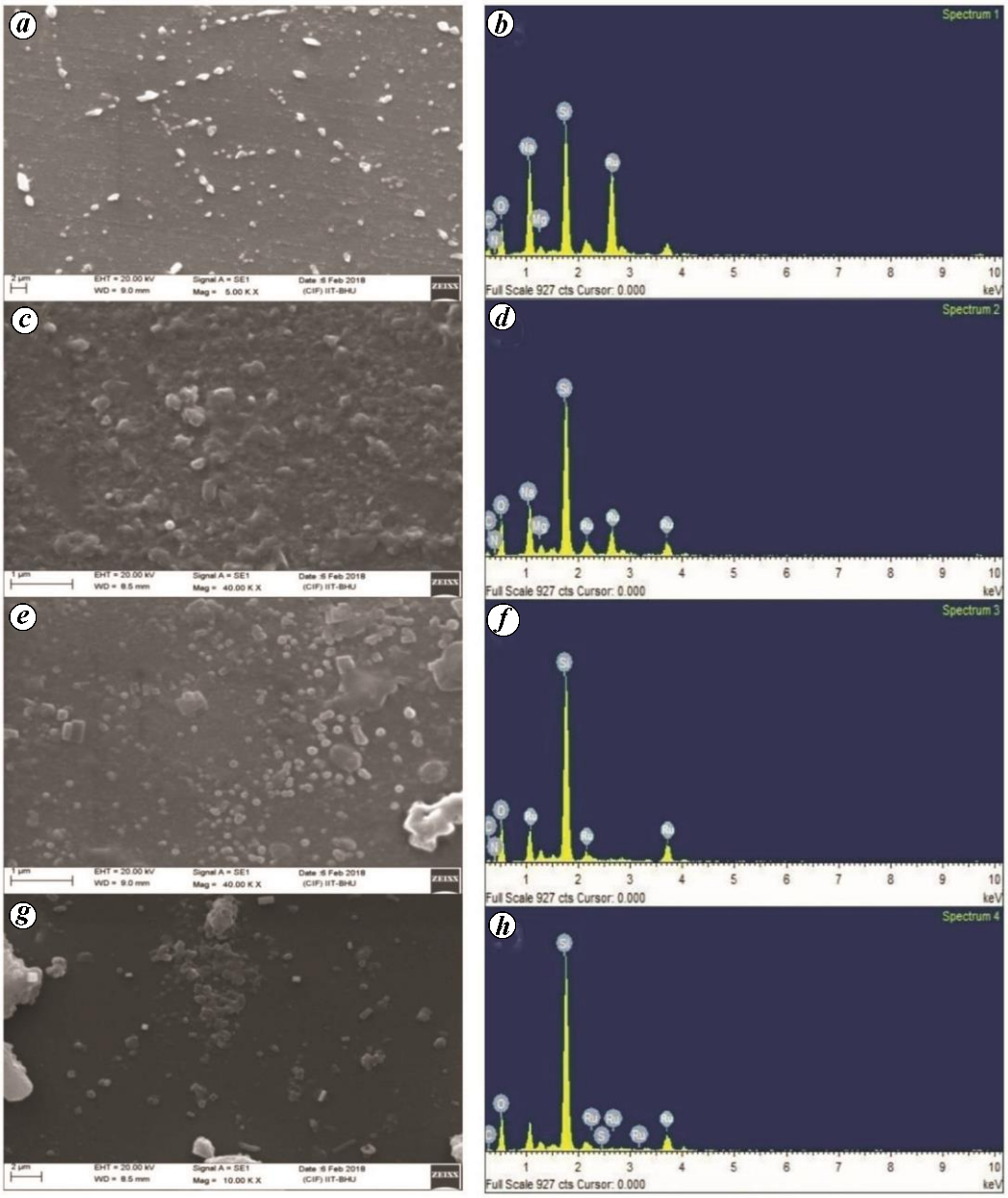

Figure 3. The images (***a***), (***c***), (***e***) and (***g***) are SEM images of RMCRL, RMCLL, RMNBL and RMOTL respectively, performed over the scale of 1–2 μm. The images (***b***), (***d***), (***f***) and (***h***) are the EDX images of RMCRL, RMCLL, RMNBL and RMOTL respectively, performed over a range of 1–10 KeV.

and chlorophyll (~665 nm) were noticed and thus supporting the stoichiometric reduction of Ru^{+3} to Ru NPs.

Further, the synthesized Ru NPs were characterized using fluorescence spectroscopy, to study fluorescence offered by them. Combined fluorescence spectrum of plant extracts and their NPs are shown in Figure 2 *b*. Remarkably, plant extracts showed fluorescence peaks in green (~561 nm, 585 nm) and red region (~612 nm, 673.5 nm) owing to fluorescence from β-carotene derivatives and chlorophyll, respectively. The fluorescence intensity from plant extracts was reduced on the formation of Ru NPs. However, this decrease is minimum in red region (673 nm), but prominent in green region, hence supporting the tentative role of chlorophyll. Figure 2 *c*, depicts serrated patterns spectra of $RuCl_3$ unlike the spectra of plant extracts. These serrations are due to capping of some phyto-organic molecules from the plant extracts on the surface of Ru NPs[39].

Infrared spectroscopic (FTIR) studies showed peaks of asymmetric –OH stretching vibration at 3500–3400 cm^{-1}. The absorption peaks at (cm^{-1}) 2845–2950, 1600–1800, 1590–1620, 1250 and at 1050–1000 were assigned to stretching vibrations due to ν(C–H), ν(C=C), ν(C=N), ν(C–O) and ν(C–O–C) respectively. Peak at ~830 cm^{-1}

corresponds to ν(C–H) bending vibration. FTIR spectra of Ru NPs displayed similar peaks but ν(C=N) vibration shifted to higher frequency. An additional peak at 479–590 cm^{-1} was obtained for metallic Ru[24]. These results (Supplementary Figure 1) support the reduction of Ru^{+3} to Ru^0 via oxidation of imine moieties, present in chlorophyll.

Powder XRD studies were done using Ru NPs-coated cover-slips. All four Ru NPs depicted major peaks (Supplementary Figure 2) at 12.71° (111), 26.69° (320), 34.38° (332) and 40.50° (521). The lattice of Ru NPs were found to be simple cubic in nature, and lattice constants (d-spacing, a, b, c, α, β, γ and c/a ratio) were deduced to be 8.55 nm, 14.81 nm, 14.81 nm, 14.81 nm, 90°, 90°, 90° and 1.00 respectively. Size of Ru NPs was calculated using Debye Scherrer equation[40]

$$\tau = \frac{K\lambda}{\beta \cos\theta}, \tag{5}$$

where τ is the particle size (nm), $K = 0.9$, λ the standard X-ray wavelength equal to 1.5406 Å, β the full width at half of the maximum (radian) and θ is the Bragg's angle. Broad and low intensity peaks of XRD supported the formation of nanosized Ru NPs, and their sizes were in the range of 10–30 nm. Additional unassigned peaks, as observed for Ag/Au NPs[41], may be attributed to deposition of some phyto-inorganic substance on the surface of NPs.

A morphological and constituent related study of Ru NPs was done by SEM and EDX. SEM images (Figure 3 *a*, *c*, *e* and *g*) showed Ru NPs of different morphologies, with particles size in the order of 30 nm. This may be due to magnetically induced agglomerations. In addition, EDX shows abundance of metallic ruthenium as displayed in Figure 3 *b*, *d*, *f*, *h*. EDX spectrum shows the presence of expected elements such as C, O, Mg, Al, P, S, Na along with Ru (at 2–3 KeV). The peaks are due to bio-capping agents which played a role in the stabilization of Ru NPs. Scanning of the glass slides poses a problem of a high intensity peak of silicon at 2.6 KeV.

Particle size and morphology of Ru NPs were further confirmed by TEM studies as shown in Figure 4 *a*, *d*, *g* and *j*. Particle size was calculated using ImageJ[41]. Ru NPs were non-uniform to spherical in morphology with a narrow particle size ranging between 19.6 and 26.5 nm (Table 1). RMCRL were of irregular morphology and were less agglomerated, but RMCLL were spherical and were non-agglomerated. RMOTL and RMNBL were hexagonal in shape with no agglomeration and had smallest particle size amongst all other Ru NPs. The SAED analysis of NPs displayed dispersity (Figure 4 *h*) and others displayed crystallinity (Figure 4 *b*, *e* and *k*). RMNBL was amorphous, but RMCRL was found to be crystalline. Unlike the other two RMCLL and RMOTL were poly-nano-crystalline. Inter-planar distances (d) were calculated by using Crystbox[42] and found to be in the range of 14.5–14.8 nm, equivalent to the value calculated from XRD spectra.

The Ru NPs have been synthesized using several plant extracts and their pharmaceutical and antibacterial activities have also been reported. To the best of our knowledge, no antifungal and antioxidant activities have been reported so far. Chemical characterization done so far supported the capping of Ru NPs by bioactive compounds found in the plant extracts. Biological characterizations were done to investigate antifungal and antioxidant properties of Ru NPs. Plant extracts showed significant antifungal activity with complete growth inhibition at 2000 µl. However, biosynthesized Ru NPs showed enhanced antifungal activity with complete growth inhibition at ~1000 µl. RMNBL shows maximum antifungal activity with complete growth inhibition at 800 µl (Supplementary Figure 3). 50% inhibitory values of all the Ru NPs were also calculated and compared (Table 2).

Antioxidant activity of Ru NPs was investigated by performing DPPH, ABTS, SO and OH radical scavenging assays. A series of solutions were prepared by adding fixed amount of radical/radical generators to increasing concentrations of Ru NPs and percent radical scavenging activity of Ru NPs was estimated for each of the samples and finally, value for a IC_{50} particular Ru NPs was evaluated (Table 3). DPPH radical scavenging activity (Supplementary Figure 4 *a*), although less than that of ascorbic acid, was still significant. The scavenging activities of RMOTL and RMCRL were higher as compared to RMCLL and RMNBL. A more sensitive ABTS radical scavenging activity (Supplementary Figure 4 *b*) was analysed. The activity was less than that of butylated hydroxyl toluene (BHT), but still significant. The scavenging activities of RMOTL and RMCRL were higher as compared to RMCLL and RMNBL. Superoxide radical scavenging activity (Supplementary Figure 4 *c*) was less than that of quercetin, but still significant. The SO radical scavenging activities of RMCRL and RMOTL were higher as compared to RMCLL and RMNBL. Hydroxyl radical scavenging activity (Supplementary Figure 4 *d*) was comparable to that of quercetin. The OH radical scavenging activities of RMOTL and RMNBL were higher compared to RMCRL and RMCLL.

Tentative mechanism

The methanolic extract of the plant leaves used for the study is known to have significant amounts of polyphenols and aromatic conjugated hydrocarbons[27–30]. Leaf extracts of *Ocimum tenuiflorum* consists of eugenol, apigenin and rosmarinic acids[43]. Tannins and terpenoids, are present in leaves of fern and *Cycas*[44]. Leaf extracts of *Catharanthus roseus* bear a variety of flavonoids and alkaloids[45]. These compounds get transferred to solvent

Table 1. The particle size and other physical parameters of ruthenium nanoparticles (Ru NPs)

Ru NPs	Morphology	Lattice	Nature	Dispersity	Average particle size (nm)
RMCRL	Irregular	Cubical	Crystalline	Mono dispersed	19.634
RMCLL	Spherical	Cubical	Polynanocrystalline	Mono dispersed	26.526
RMNBL	Hexagonal	Cubical	Amorphous	Mono dispersed	25.962
RMOTL	Orthorhombic	Cubical	Polynanocrystalline	Mono dispersed	20.928

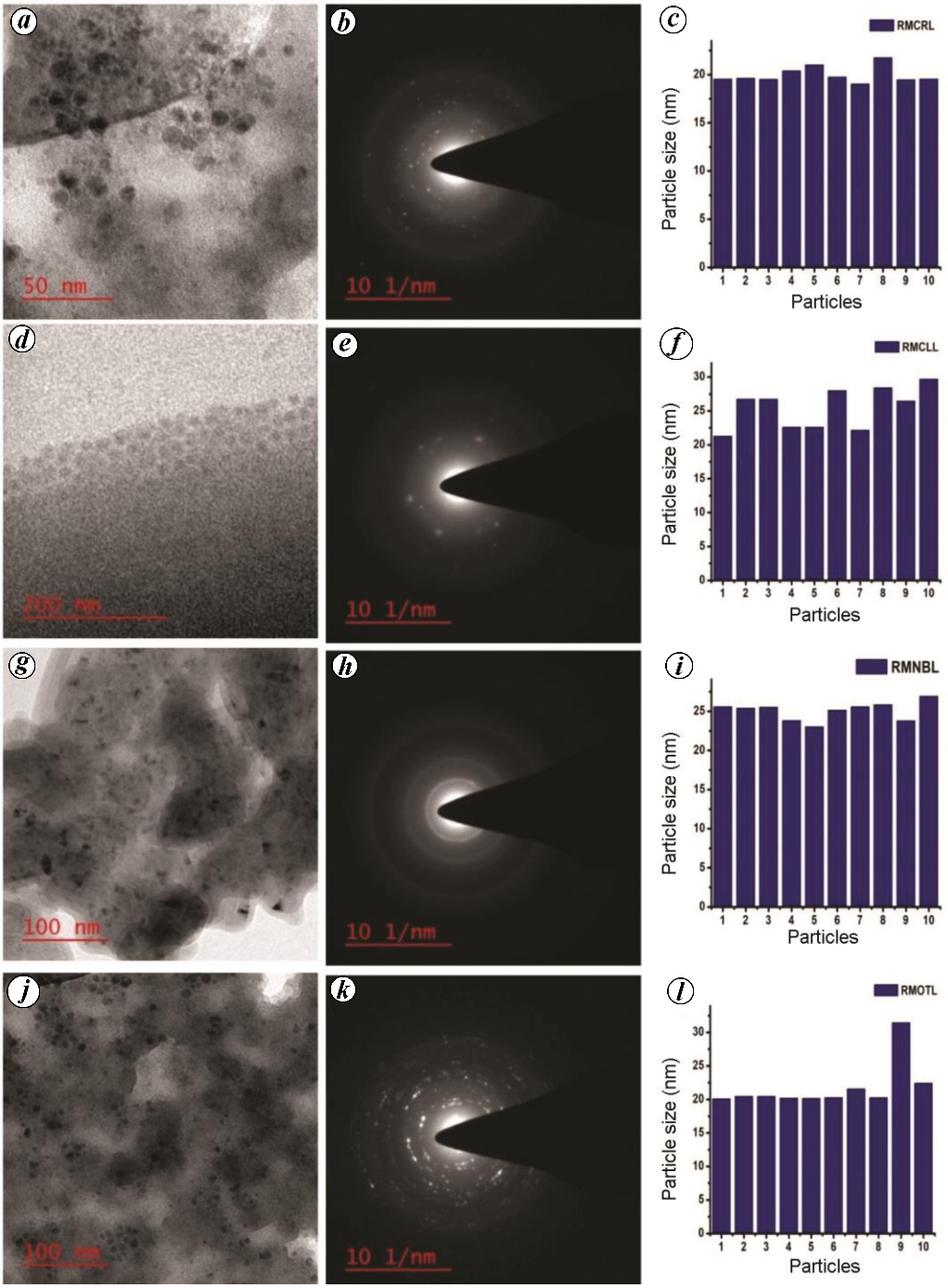

Figure 4. TEM and SAED images of synthesized Ru NPs. Images (***a***), (***d***), (***g***) and (***j***) represent TEM images of RMCRL, RMCLL, RMNBL and RMOTL respectively. (***b***), (***e***), (***h***) and (***k***) represent SAED images of RMCRL, RMCLL, RMNBL and RMOTL respectively. The particle size distribution represented as bar diagram over 10 significant Ru NPs in images of RMCRL, RMCLL, RMNBL and RMOTL are depicted in (***c***), (***f***), (***i***) and (***l***) respectively.

phase during extract preparation and are responsible for the formation of Ru NPs, and their stabilization. Ru^{3+} ions mediate oxidation of polyphenols to less stable ortho-benzoquinone derivatives; gets reduced to Ru^0 (Supplementary Figure 5) that nucleates into nano-crystalline and amorphous NPs that are stabilized by various bioactive compounds. A significant decrease in the ν(O–H) stretching vibration supports this conclusion (Supplementary Figure 1 *a–d*).

Correlation plots

The present study was initiated with an assumption that the particle size and biological activity of the Ru NPs could be correlated. Enhanced antibacterial and antioxidant activity with a decrease in size of metal NPs have already been reported[46]. The reduced particle size and increased surface area enhances surface activity, and the increased surface area would offer more vacancy for stabilization. If plant extract mediated synthesis approach is followed, bioactive compounds of the extract would cap over NPs surface. However, variation of plant species can significantly affect this process, as a particular type of biological activity of a plant is specific to itself and its effectiveness varies from plant to plant. Irrespective of their size and shape, NPs synthesized through a particular plant extract will show similar stress enduring properties as shown by the plant itself, which may not be shown by other NPs synthesized by extracts of other plants. Moreover, this property would vary irrespective of NPs size and surface.

Various plant groups are required for establishing a strong correlation of their NPs particle size and biological activity. This information would be useful for developing new Ru NPs as per our desire. These biological properties vary largely over diverse plant groups namely angiosperms (*Catharanthus roseus* and *Ocimum tenuiflorum*), gymnosperms (*Cycas revoluta*) and pteridophytes (*Nephrolepis biserrata*). Rare availability, excessive labour and by-product generation are reasons for avoiding thallophytes and bryophytes. Two angiosperms were employed in order to represent the diversity of this plant group. Ferns (pteridophytes) are more primitive to angiosperms with more stress and infection enduring properties due to their genetic ability to generate several stress and infection enduring proteins and secondary metabolites[47]. Irrespective of pteridophytes and angiosperms, gymnosperms show less biological activity, restricted only to some species and compounds such as tannins found in them which are allergic in nature[48]. The species selected here have no specific biological activity, and are more primitive compared to biologically important gymnosperms like *Taxus* and *Ephedra*.

Different biological activities were correlated to log of particle size (in nm), biological activity parameter (50% inhibitory and IC_{50} values) and plant evolutionary line, for better and comparative study (Supplementary Tables 1 and 2 respectively). These plots were collectively called the NPs-Pg correlation plot (Supplementary Figure 5). Broadly, two types of plots were obtained. According to our expectation, NPs-Pg plots showed biological inactivity of RMCLL which was common, and much of the biological complexities were concerned only to RMCRL, RMOTL and RMNBL. The NPs-Pg plot for antifungal activity and HSA assay, i.e. (NPs-Pg@AFA/LD_{50}) and (NPs-Pg@HSA/IC_{50}) respectively, support better antifungal and hydroxide scavenging activity at lower particle size. Plants such as *Nephrolepis biserrata*, are supposed to have better LD_{50} as compared to others, and so does their nanoparticles. Notable antifungal activities were also displayed by RMCRL and RMOTL (Supplementary Figure 6 *a*, *e* respectively). The NPs-Pg plot for DPPHS, ABTSS and SORS assays, i.e. (NPs-Pg@DPPHS/IC_{50}), (NPs-Pg@ABTSS/IC_{50}) and (NPs-Pg@SORS/IC_{50}) (Supplementary Figure 6 *b–d*) supported that RMCRL and RMOTL were efficient in radical scavenging assays, giving hint that better antioxidant properties can be achieved through NPs synthesized by modern taxonomic families. In these plots, a minimum value is obtained in between RMCRL and RMOTL suggesting a scope of attaining better antioxidant properties through NPs synthesized by plant species found in the families in between apocynaceae and labiatae. Maintaining a standard synthesis and characterization protocol is necessary for comparison. Although this technique is crude, yet it develops predictability for such a diverse mode of synthesis.

Table 2. Antifungal activity of Ru NPs (compared with 50% inhibitory (ml) value of 2.4 mM $RuCl_3$ = 2.0)

Plant extract	50% inhibitory (ml)	Ru NPs	50% inhibitory (ml)
MCRL	1.5	RMCRL	0.8
MCLL	1.5	RMCLL	0.9
MNBL	1.5	RMNBL	0.6
MOTL	1.5	RMOTL	0.8

Table 3. IC_{50} values of antioxidant activity

	IC_{50} values of antioxidant activities (mg/ml)			
Ru NPs	DPPHS	ABTSS	SORS	HSA
RMCLL	0.692	0.886	1.165	2.391
RMCRL	0.395	0.676	0.569	1.456
RMNBL	0.986	0.852	1.265	1.389
RMOTL	0.389	0.626	0.936	1.246

Conclusion

In the present study we have synthesized simple cubic Ru NPs (monodispersed) through the green protocol

using plant extracts. This protocol of green synthesis has been established owing to multifunctional nature of Ru NPs and being environment friendly. The present study has utilized plants of medicinal importance in order to establish significant bioactivity. The biological characterizations of the NPs have been carried out under strict sterilized conditions and the results have been compared with each other. These NPs have been executed in antioxidative and antifungal activities. The studies on antifungal and antioxidation was a new approach in the area of Ru NPs that gave satisfactory results. However, the heart of this study lies in the presumptions of a tentative correlation amongst NPs size, biological activity and phylogeny, which were further confirmed by novel NPs-Pg plots devised for easy comparison and inference from the obtained results. These plots were not only capable of discussing this study, but also showed a way to predict those plants that could give much promising results.

Conflicts of interests: The authors declare no conflict of interest. All experimental works were carried out by Pranshu Gupta.

Supplementary material: Images related to tentative reaction mechanism (Supplementary Figure 1), infrared spectra (Supplementary Figure 2), combined powder-XRD spectra (Supplementary Figure 3), data and image of antifungal activities (Supplementary Table 1, Figure 4), IC_{50} values of antioxidant activities (Supplementary Table 2) and data with correlation plots (Supplementary Table 3, Figure 5) are presented as supplementary data.

1. Iravani, S., Green synthesis of metal nanoparticles using plants. *Green Chem.*, 2011, **13**, 2638–2650.
2. Akbarian, M., Mahjoub, S., Elahi, S. M., Zabihi, E. and Tashakkorean, H., *Urtica dioica* Linn. extracts as a green catalyst for the biosynthesis of zinc oxide nanoparticles: characterization and cytotoxic effects on fibroblast and MCF-7 cell lines. *New J. Chem.*, 2018, **42**, 5822–5833.
3. Oliver, S., Wagh, H., Liang, Y., Yang, S. and Boyer, C., Enhancing the antimicrobial and antibiofilm effectiveness of silver nanoparticles prepared by green synthesis. *J. Mater. Chem.*, 2018, **6**, 4124–4138.
4. Mittal, A. K., Chisti, Y. and Banerjee, U. C., Synthesis of metallic nanoparticles using plant extracts. *Biotechnol. Adv.*, 2013, **31**, 346–356.
5. Ahmed, S., Ahmed, M., Swami, B. L. and Ikram, S., A review on plants extract mediated synthesis of silver nanoparticles for antimicrobial applications: a green expertise. *J. Adv. Res.*, 2016, **7**, 17–28.
6. Raj, R. A., Al Salhi, M. S. and Devanesan, S., Microwave-assisted synthesis of nickel oxide nanoparticles using *Coriandrum sativum* leaf extract and their structural-magnetic catalytic properties. *Materials*, 2017, **10**, 460–472.
7. Pandian, C. J., Palanivel, R. and Dhananasekaran, S., Green synthesis of nickel nanoparticles using *Ocimumsanctum* and their application in dye and pollutant adsorption. *Chinese J. Chem. Eng.*, 2015, **23**, 1307–1315.
8. Zuverza-Mena, N., Medina-Velo, I. A., Barrios, A. C., Tan, W., Peratta-Videa, J. R. and Gardea-Torresdey, J. L., Copper nanoparticles/compounds impact agronomic and physiological parameters in cilantro (*Coriandrum sativum*). *Environ. Sci.-Proc. Imp.*, 2015, **17**, 1783–1793.
9. Shobha, G., Moses, V. and Anand, S., Biological synthesis of copper nanoparticles and its impact – a review. *Int. J. Pharm. Sci. Invent.*, 2014, **3**, 28–38.
10. Chen, G. *et al.*, Hollow ruthenium nanoparticles with small dimensions derived from Ni@Ru core@shell structure: synthesis and enhanced catalytic dehydrogenation of ammonia borane. *Chem. Comm.*, 2012, **48**, 8009–8011.
11. Kang, J., Zhang, S. and Zhang, Q., Ruthenium nanoparticles supported on carbon nanotubes as efficient catalysts for selective conversion of synthesis gas to diesel fuel. *Angew. Chem. Int. Ed.*, 2009, **48**, 2565–2568.
12. Gupta, S., Giordano, C. and Gradzielski, M., Microwave-assisted synthesis of small Ru nanoparticles and their role in degradation of congo red. *J. Colloid. Interf. Sci.*, 2013, **411**, 173–181.
13. Yang, S., Besson, M. and Descorme, C., Catalytic wet air oxidation of succinic acid over Ru and Pt catalysts supported on $Ce_xZr_{1-x}O_2$ mixed oxides. *Appl. Catal. B: Environ.*, 2015, **165**, 1–9.
14. Veerakumar, P., Ramdass, A. and Rajagopal, S., Ruthenium nanocatalysis on redox reactions. *J. Nanosci. Nanotechnol.*, 2013, **13**, 4761–4786.
15. Dikhtiarenko, A., Khainakov, S. A. and de Pedro, I., Series of 2D heterometallic coordination polymers based on ruthenium(III) oxalate building units: synthesis, structure, and catalytic and magnetic properties. *Inorg. Chem.*, 2013, **52**, 3933–3941.
16. Sahu, M., Shaikh, M., Khilari, S. and Ranganath, K. V., Ruthenium nanoparticles stabilized on nano magnesium oxide in the presence of ionic liquids: a highly active and efficient electrocatalyst for hydrogen evolution reaction. *Catal. Green Chem. Eng.*, 2017, **1**, 1–7.
17. Gericke, D. *et al.*, Green catalysis by nanoparticulate catalysts developed for flow processing: case study of glucose hydrogenation. *RSC Adv.*, 2015, **21**, 1–6.
18. Hemraj-Benny, T., Tobar, N., Carrero, N. and Sumner, R., Microwave assisted green synthesis of ruthenium nanoparticles supported on non functional single walled carbon nanotubes for congo red dye degradation. *Mater. Chem. Phys.*, 2018, **216**, 72–81.
19. Zhao, J., Hu, W., Li, H., Ji, M., Zhao, C., Wang, Z. and Hu, H., One-step green synthesis of a ruthenium/graphene composite as a highly efficient catalyst. *RSC Adv.*, 2015, **5**, 7679–7686.
20. Dikhtiarenko, A., Khainakov, S. A., Khaynakova, O., García, J. R. and Gimeno, J., High-yielding green hydrothermal synthesis of ruthenium nanoparticles and their characterization. *J. Nanosci. Nanotechnol.*, 2016, **6**, 6139–6147.
21. Hussain, I., Singh, N. B., Singh, A., Singh, H. and Singh, S. C., Green synthesis of nanoparticles and its potential application. *Biotechnol. Lett.*, 2015, **38**, 548–560.
22. Srivastava, S. K. and Constanti, M., Room temperature biogenic synthesis of multiple nanoparticles (Ag, Pd, Fe, Rh, Ni, Ru, Pt, Co and Li) by *Pseudomonas aeruginosa* SM1. *J. Nanopart. Res.*, 2012, **14**, 831–841.
23. Ali, M. S., Anuradha, V., Abishek, R., Yogananth, N. and Sheeba, H., *In vitro* anticancer activity of green synthesis ruthenium nanoparticle from *Dictyota dichotoma* marine algae. *Nano World J.*, 2017, **3**, 66–71.
24. Gopinath, K., Karthika, V. and Gowri, S., Antibacterial activity of ruthenium nanoparticles synthesized using *Gloriosa superb* Linn. leaf extract. *J. Nanostruct. Chem.*, 2014, **4**, 83–89.
25. Kannan, S. K. and Sundrarajan, M., Green synthesis of ruthenium oxide nanoparticles: characterization and its antibacterial activity. *Adv. Powder Technol.*, 2015, **26**, 1505–1511.
26. Zhang, Z., Suo, Y., He, J., Li, G., Hu, G. and Zheng, Y., Selective hydrogenation of ortho-chloronitrobenzene over biosynthesized ruthenium–platinum bimetallic nanocatalysts. *Ind. Eng. Chem. Res.*, 2016, **55**, 7061–7068.

27. Pattanayak, P., Behera, P. and Das, D., Ocimum sanctum Linn. A reservoir plant for therapeutic applications: an overview. *Pharmacogn. Rev.*, 2010, **4**, 95–105.
28. Ahmad, N. H., Rahim, R. A. and Mat, I., *Catharanthus roseus* aqueous extract is cytotoxic to jurkat leukaemic T-cells but induces the proliferation of normal peripheral blood mononuclear cells. *Trop. Life Sci. Res.*, 2010, **21**, 101–113.
29. Kumar, B. S. and Kumar, V., Antimicrobial and antioxidant activity of *Cycas circinalis* Linn. and *Ionidium suffruticosum* Ging. *Innov. J. Med. Sci.*, 2017, **5**, 12–14.
30. Ibrahim, B., Nkoulémbéné, C. A., Mounguengui, S., Lépengué, A. N. and Azizet, Y. I., Antihypertensive potential of aqueous extract of *Nephrolepis biserrata* leaves on toad aorta. *Med. Aromat. Plants*, 2015, **5**, 220–228.
31. Holzwarth, U. and Gibson, N., The Scherrer equation versus the Debye–Scherrer equation. *Nat. Nanotechnol.*, 2011, **6**, 534–534.
32. Balouiri, M., Sadiki, M. and Ibnsouda, S. K., Methods for *in vitro* evaluating antimicrobial activity: a review. *J. Pharmaceut. Anal.*, 2016, **6**, 71–79.
33. Kedare, S. P. and Singh, R. P., Genesis and development of DPPH method of antioxidant assay. *J. Food Sci. Technol.*, 2011, **48**, 412–422.
34. Re, R., Pellegrini, N. and Proteggente, A., Antioxidant activity applying an improved ABTS radical cation decolorization assay. *Free Radical. Biol. Med.*, 1999, **26**, 1231–1237.
35. Hazra, B., Biswas, S. and Mandal, N., Antioxidant and free radical scavenging activity of *Spondias pinnata. BMC Complem. Altern. Med.*, 2008, **8**, 63–63.
36. Thomas, C., Mackey, M. M. and Diaz, A. A., Hydroxyl radical is produced via the Fenton reaction in sub-mitochondrial particles under oxidative stress: implications for diseases associated with iron accumulation. *Redox Rep.*, 2009, **14**, 102–108.
37. Chen, W., Ghosh, D. and Sun, J., Dithiocarbamate-protected ruthenium nanoparticles: synthesis, spectroscopy, electrochemistry and STM studies. *Electrochim. Acta*, 2007, **53**, 1150–1156.
38. Thrane, J. E., Kyle, M. and Striebel, M., Spectrophotometric analysis of pigments: a critical assessment of a high-throughput method for analysis of algal pigment mixtures by spectral deconvolution. *PLoS ONE*, 2015, **10**, 1–24.
39. Parashar, U. K., Saxena, P. S. and Srivastava, A., Bioinspired synthesis of silver nanoparticles. *Dig. J. Nanomater. Bios.*, 2009, **4**, 159–166.
40. Zhou, Y. C. and Rahaman, M. N., Hydrothermal synthesis and sintering of ultrafine CeO_2 powders. *J. Mater. Res.*, 1993, **8**, 1680–1686.
41. Abramoff, M. D., Magelhaes, P. J. and Ram, S. J., Image processing with ImageJ. *Biophoton. Int.*, 2004, **11**, 36.
42. Klinger, M. and Aleš, J., Crystallographic tool box (CrysTBox): automated tools for transmission electron microscopists and crystallographers. *J. Appl. Crystallogr.*, 2015, **48**, 1107.
43. Baliga, M. S., Jimmy, R. and Thilakchand, K. R., *Ocimum Sanctum* Linn. (holy basil or Tulsi) and its phytochemicals in the prevention and treatment of cancer. *Nutr. Cancer*, 2013, **65**, 26–35.
44. Ahmad, E., Arshad, M. and Khan, M. Z., Secondary metabolites and their multidimensional prospective in plant life. *J. Pharmacogn. Phytochem.*, 2017, **6**, 205–214.
45. Kumar, R., Ragunathan, R. and Kabesh, K., Phytochemical analysis of *Catharanthus roseus* plant extract and its antimicrobial activity. *Int. J. Pure Appl. Biosci.*, 2015, **3**, 162–172.
46. Beer, H., Staehelin, T., Douglas, H. and Braude, A. I., Relationship between particle and biological activity of *E. coli* Boivin endotoxin. *J. Clin. Invest.*, 1965, **44**, 592–602.
47. Sahayaraj, K., Borgio, J. F. and Raju, G., Antifungal activity of three fern extracts on causative agents of groundnut early leaf spot and rust diseases. *J. Plant Prot. Res.*, 2009, **49**, 1–4.
48. Volpicella, M., Leoni, C., Fanizza, I., Placido, A., Pastorello, E. A. and Ceci, L. R., Overview of plant chitinases as food allergens. *J. Agric. Food Chem.*, 2014, **62**, 5734–5742.

ACKNOWLEDGEMENTS. We thank CAS and Nanomission programmes of the Department of Chemistry, BHU, for chemicals and instrumental facilities. We also thank Dr Preetam Singh, Department of Ceramic Engineering, IIT, BHU, for his help in micro-structural studies, such as SEM, TEM, EDX and SAED analysis of nanoparticles.

Received 25 February 2019; revised accepted 18 July 2019

doi: 10.18520/cs/v117/i8/1308-1317